



This is a repository copy of *Anisotropic Approach for Simulating Electron Transport in Layered Materials: Computational and Experimental Study of Highly Oriented Pyrolytic Graphite*.

White Rose Research Online URL for this paper:
<http://eprints.whiterose.ac.uk/130882/>

Version: Accepted Version

Article:

Azzolini, M., Morresi, T., Abrams, K. orcid.org/0000-0002-2789-7204 et al. (6 more authors) (2018) Anisotropic Approach for Simulating Electron Transport in Layered Materials: Computational and Experimental Study of Highly Oriented Pyrolytic Graphite. *Journal of Physical Chemistry C*, 122 (18). pp. 10159-10166. ISSN 1932-7447

<https://doi.org/10.1021/acs.jpcc.8b02256>

Reuse

Items deposited in White Rose Research Online are protected by copyright, with all rights reserved unless indicated otherwise. They may be downloaded and/or printed for private study, or other acts as permitted by national copyright laws. The publisher or other rights holders may allow further reproduction and re-use of the full text version. This is indicated by the licence information on the White Rose Research Online record for the item.

Takedown

If you consider content in White Rose Research Online to be in breach of UK law, please notify us by emailing eprints@whiterose.ac.uk including the URL of the record and the reason for the withdrawal request.



eprints@whiterose.ac.uk
<https://eprints.whiterose.ac.uk/>

An anisotropic approach for simulating electron transport in layered materials: computational and experimental study of Highly Oriented Pyrolytic Graphite

Martina Azzolini,^{*,†,‡} Tommaso Morresi,^{†,‡} Kerry Abrams,[¶] Robert Masters,[¶]
Nicola Stehling,[¶] Cornelia Rodenburg,[¶] Nicola M. Pugno,^{‡,§,||} Simone Taioli,^{†,⊥}
and Maurizio Dapor^{*,†}

[†]*European Centre for Theoretical Studies in Nuclear Physics and Related Areas
(ECT*-FBK) and Trento Institute for Fundamental Physics and Applications
(TIFPA-INFN), Trento, Italy*

[‡]*Laboratory of Bio-Inspired and Graphene Nanomechanics, Department of Civil,
Environmental and Mechanical Engineering, University of Trento, Italy*

[¶]*Department of Material Science and Engineering, University of Sheffield, United Kingdom*

[§]*Ket-Lab, Edoardo Amaldi Foundation, Italian Space Agency, Rome, Italy*

^{||} *School of Engineering and Materials Science, Queen Mary University of London, United
Kingdom*

[⊥]*Faculty of Mathematics and Physics, Charles University, Prague, Czech Republic*

E-mail: mazzolini@ectstar.eu; dapor@ectstar.eu

Abstract

Highly Oriented Pyrolytic Graphite presents a layered structure. In this work, we propose a theoretical and computational model for taking into account the anisotropic structure of graphite in the Monte Carlo simulations of charge transport. In particular, the dielectric characteristics, such as the inelastic mean free path and energy losses, are treated by linearly combining the contribution to these observables along the two main orthogonal directions identifying the crystalline structure (along the layer plane and perpendicular to it). Energy losses are evaluated from *ab initio* calculations of the dielectric function of the system along these two perpendicular directions. Monte Carlo simulated spectra, obtained with this approach, are compared with acquired experimental data of Reflection Electron Energy Loss and Secondary Electron spectra showing a good agreement. These findings validate the idea of the importance of considering properly-weighted inter-planar and intra-planar interactions in the simulation of electron transport in layered materials.

Introduction

Carbon-based materials have recently attracted significant attention due to the discovery of new exciting science, particularly in connection with the unique band structure of graphene. Within this 2D material, in which the planar topology is realized by a sp^2 -net of carbon atoms, electrons behave like relativistic fermions offering the potential for high speed nanoscale electronics and for replacing silicon in light-weight and wearable devices. Other carbon allotropes, obtained for example by rolling up graphene in carbon nanotubes, display further interesting properties, as they can be produced with both semiconducting and metallic character depending on the twist and on the diameter of the tube.^{1,2} Nevertheless, these materials are still difficult to be synthesized in a cost-effective, scalable way.

At variance with other allotropes of carbon, graphite can be naturally found (the others two being amorphous carbon and diamond). Thus, it is worthy to explore its properties,

particularly with respect to its electronic characteristics for applications in opto-electronic devices and imaging. Graphite represents a 3D stacking of graphene sheets, and thus display an uniaxial layered structure which retains some characteristics of graphene, while its thermal, acoustic and electronic properties are highly anisotropic. Most notably, the large anisotropy of the electric conductivity means that along the planes graphite shows an higher conductivity than in the direction normal to the surface³.

In this work we present Monte Carlo (MC) simulations of Reflection Electron Energy Loss (REEL) and Secondary Electron (SE) spectra of Highly Oriented Pyrolytic Graphite (HOPG) taking into account the target anisotropic structure. Simulated spectra are compared with experimental data recorded in our laboratories. In this model, elastic scattering events between electrons and target atoms are treated via the Mott theory⁴, which is based on the solution of the Dirac equation in a central field. At variance, inelastic collisions between the primary electron beam and the electron cloud of the target can result in the excitation of bulk and surface plasma oscillations. In this regard, an accurate description of the electron energy loss is provided by the dielectric theory developed by Ritchie⁵. Within this approach, the key quantity for the calculation of the inelastic cross section is the Energy Loss Function (ELF), defined as the imaginary part of the inverse of the dielectric function $\epsilon(\vec{q}, W)$, where \vec{q} is the transferred momentum owing to the inelastic interactions and W is the energy loss. To take into account graphite anisotropy, we assess from *ab initio* time-dependent density functional simulations the dielectric function optical limit ($\epsilon_{\vec{q} \rightarrow 0}$) along two orthogonal directions: along the direction normal to the layer (identified by the vector \vec{c}), which accounts for inter-planar interactions, and along that one perpendicular to \vec{c} , which describes intra-planar excitations (in-plane direction). Finally, the ELFs, obtained by combining these two dielectric functions, were fitted in the optical limit by using Drude–Lorentz functions, and extended to finite momenta by a dispersion law obtained within the Random Phase Approximation (RPA)⁶. In this way, the energy losses in both planar and inter-planar directions were taken into account appropriately in our Monte Carlo simulations.

In the following sections the Monte Carlo model as well as the experimental procedures will be described in details. Then the comparison between experimental and simulated spectra will be presented.

Experimental Details

Reflection Electron Energy Loss Spectra Acquisition

The sample of HOPG was initially cleaved ex-situ, and then was cleaned by annealing at 600 °C for 10 min in ultra-high vacuum. The REEL measurements were realized at a base pressure of $\approx 2 \times 10^{-2}$ mbar in a PHI 545 system. The experimental apparatus is composed by a coaxial electron gun, a non-monochromatic MgK α ($h\nu = 1253.6$ eV) X-ray source, a He discharge lamp and double-pass cylindrical mirror analyser (CMA). In CMA, the angle between primary electron beam and the surface normal is maintained constant, while emitted electrons cross the surface in different directions that are described by the angle between the surface normal and the CMA axis (30°), the entrance angle to the analyser ($42^\circ \pm 6^\circ$) and the azimuth angle in a plane normal to the CMA axis. The energy resolution was maintained constant at 0.6 eV, as measured on a Pd Fermi edge. The zero-loss peak has a measured full width half maximum of 0.9 eV. The energy of the impinging electron beam spans the range from 250 eV to 2000 eV. The acquired spectra are corrected for the energy dependence ($E^{-0.9}$) accordingly to the analyser transmission function.

Secondary Electron Spectrum Acquisition

SE spectrum acquisition was performed with a FEI Helios NanoLab G3 UC scanning electron microscope (SEM). HOPG with a mosaic spread of $3.5 \pm 1.5^\circ$ (purchased from Agar scientific) was mounted on an aluminium pin-stub using silver paint. Prior to specimen insertion into the SEM, the HOPG surface was mechanically exfoliated. The maximum time between exfoliation, insertion into the SEM vacuum chamber and pump down to vacuum

was less than 3 minutes. For imaging and spectra collection, the vacuum pressure at room temperature was 3×10^{-6} mbar and the working distance was kept to 4 mm. The design of the in-lens detector of this SEM allows the collection of different SE energy ranges by changing a mirror electrode voltage (M parameter). Images were collected at different M settings ranging from minimum electron energy of -0.7 to a maximum of 12.7 eV. SE spectra were collated by differentiating the mean intensity of each image from each individual M step. SE energy calibration method for this system can be found in Young et al.⁷ and the supporting information of Wan et al.⁸, whilst the absolute energy value was checked by fine structures reported experimentally in literature (3, 4 and 7.5 eV⁹) for HOPG and fine structure for diamond (6 eV¹⁰). Detection artifacts within a certain M range were identified by evaluating the average intensity of a reference gold sample with the smallest possible filter parameter step difference (0.1 V). The artefacts manifested as an increment in M without an associated signal change, signifying a discrepancy between the stated and actual M. A lookup table of corrected M was created, excluding the artefacts and re-scaling the remaining M to the initial filter parameter collection range. The differentiation of the S-curve to obtain the spectrum was performed using the corrected SE energy values associated with the respective M values.

Computational Details

Elastic Scattering

Elastic scattering between the impinging electrons and the atoms of the target is described by the Mott theory (see, for example,¹¹⁻¹⁵). The atomic potential was obtained self-consistently by solving the Dirac-Kohn-Sham equations for the carbon atom within the local-spin-density approximation (LSDA) as implemented in the ELK software program¹⁶. The elastic scattering cross-section is calculated as reported in Ref.¹⁷.

For $T = 10$ eV we find a total elastic scattering cross-section $\sigma_{\text{el}} = 28.3 \text{ \AA}^2$ and an elastic mean free path $\lambda_{\text{el}} = 0.31 \text{ \AA}$. This value of λ_{el} is one order of magnitude lower than the lat-

tice parameters of graphite ($\vec{a} = 2.46 \text{ \AA}$, $\vec{c} = 6.71 \text{ \AA}$) and is thus unphysical. Therefore, we introduce a correction to the Mott cross-section at low energy.¹⁸ Ganachaud and Mokrani¹⁹ proposed to multiply the elastic scattering cross-section σ_{el} by a cut-off function in order to diminish σ_{el} at low energy. Similarly to this model, the total elastic scattering cross-section can be obtained by multiplying the cross section calculated using the partial-wave expansion method by the following factor:

$$R(T) = \tanh(\alpha T^2) \quad (1)$$

where α is a parameter to be determined. It is worth noting that in the previous function, the α parameter is different from the α_C parameter of the Ganachaud and Mokrani cut off function. Indeed, the latter includes also the material energy band gap. By choosing $\alpha = 0.003 \text{ 1/eV}^2$ the value of the elastic mean free path for $T = 10 \text{ eV}$ is $\lambda_{\text{el}} = 1.15 \text{ \AA}$. Fig. 1 shows the behavior of σ_{el} (left panel) and λ_{el} (right panel) obtained with $\alpha = 0.003 \text{ 1/eV}^2$, along with those calculated by using the bare Mott theory. By introducing this factor, one obtains

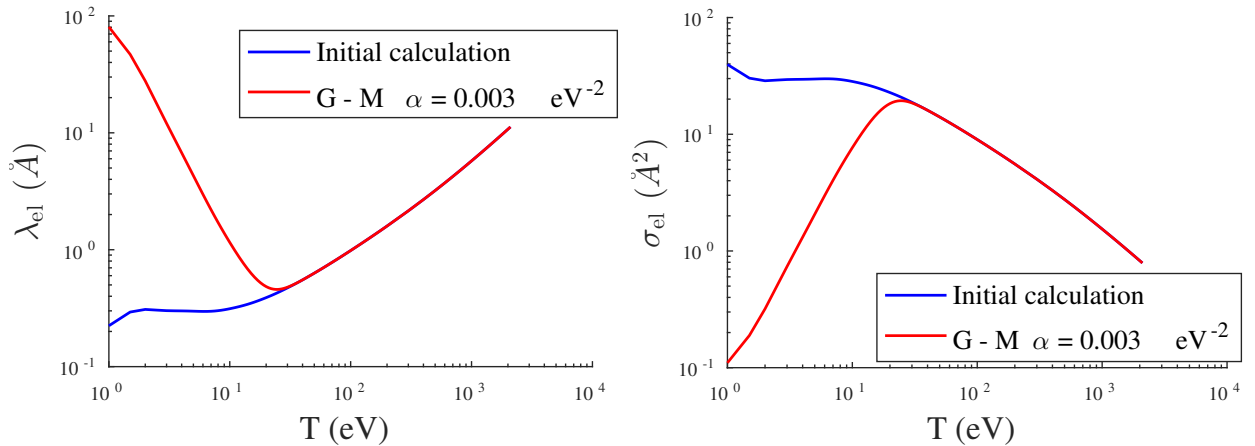


Figure 1: σ_{el} (left panel) and λ_{el} (right panel) calculated from the bare Mott theory (blue line) and by using the correction proposed by Ganachaud and Mokrani ($\alpha = 0.003 \text{ 1/eV}^2$) (red line).

a behaviour of the elastic scattering cross-section consistently decreasing at low energy.

Moreover, it was found out that the use of a cut-off function is necessary to obtain a good

agreement between calculated and experimental SE spectra.

Inelastic Scattering

The inelastic scattering between the impinging electrons and the electron clouds of the target atoms was dealt with the Ritchie theory⁵.

Within this approach, the total inelastic cross-section can be computed by assessing the inelastic mean free path λ_{inel} (IMFP). The latter can be obtained by integrating over the energy loss interval the differential inverse inelastic mean free path (DIIMF):

$$\lambda_{\text{inel}}^{-1} = \int_0^{T/2} \frac{d\lambda_{\text{inel}}^{-1}}{dW} dW \quad (2)$$

where T is the primary beam kinetic energy and the DIIMF is defined as:

$$\frac{d\lambda_{\text{inel}}^{-1}}{dW} = \frac{1}{\pi T a_0} \int_{q_-}^{q_+} \frac{dq}{q} \text{Im} \left[-\frac{1}{\epsilon(\vec{q}, W)} \right] \quad (3)$$

where a_0 is the Bohr radius. The limits of integration of the integral in Eq. (3) are set to $q_{\pm} = \sqrt{2mT} \pm \sqrt{2m(T-W)}$ for momentum conservation¹¹. The integrand in Eq. (3) is the so-called ELF.

According to Eq. (3), to model the inelastic collisions one needs to compute the dielectric function of the target material as a function of the momentum \vec{q} and of the energy transferred during the inelastic collision W . ELFs were calculated in the optical limit ($\vec{q} \rightarrow 0$) from *ab initio* simulations using the ELK code¹⁶ within the framework of Linear Response Time Dependent Density Functional Theory (LR-TDDFT). In these calculations we used a k -point sampling of $20 \times 20 \times 20$ mesh points, a cut-off for augmented plane waves equal to 400 eV, and a Fermi-smearing of 0.2 eV.

Considering the anisotropic structure of HOPG, two different orientations of energy losses were taken into account: on the one hand, we considered the transferred momentum \vec{q} parallel to the vector normal to the plane structure \vec{c} , and on the other hand \vec{q} perpendicular

to \vec{c} . Dielectric functions and derived observables, such as elastic and inelastic mean free paths, are reported for these two cases in the following discussion respectively as $\epsilon_{\parallel}(q, W)$ and $\epsilon_{\perp}(q, W)$, as well as the same notation is applied to the mean free paths λ_{\parallel} and λ_{\perp} . Optical ELF's were then fitted by Drude–Lorentz (D-L) functions as follows:

$$ELF = \sum_n \frac{A_n \Gamma_n W}{(E_n^2(q) - W^2)^2 - (\Gamma_n W)^2} \quad (4)$$

where A_n is the excitation strength of the n -th oscillator, Γ_n the damping constant, and E_n the plasmon excitation energy. In Fig. 2 *ab initio* data and final fit functions are shown, while in Tabs. 1 and 2 the fitting parameters are reported. In the fitting procedure the number of oscillators was chosen to reproduce the *ab initio* spectra. Moreover, the choice of these optimal parameters leads to fulfilling the f-sum rule.

Table 1: D–L parameters ($\vec{q} \parallel \vec{c}$ direction)

n	A_n (eV ²)	Γ_n (eV)	E_n (eV)
1	0.15	1.75	0.80
2	0.62	1.76	4.06
3	13.26	4.22	15.57
4	51.80	1.90	18.23
5	25.52	6.23	20.73
6	452.31	20.02	37.93
7	112.91	19.84	48.25

Table 2: D–L parameters ($\vec{q} \perp \vec{c}$ direction)

n	A_n (eV ²)	Γ_n (eV)	E_n (eV)
1	0.43	5.36	2.58
2	8.96	1.73	6.99
3	0.25	8.30	14.53
4	33.93	10.16	21.77
5	32.00	10.50	24.32
6	466.69	6.99	28.03
7	100.30	30.03	38.09

Finally, ELF fit functions are extended to finite values of q by applying the quadratic

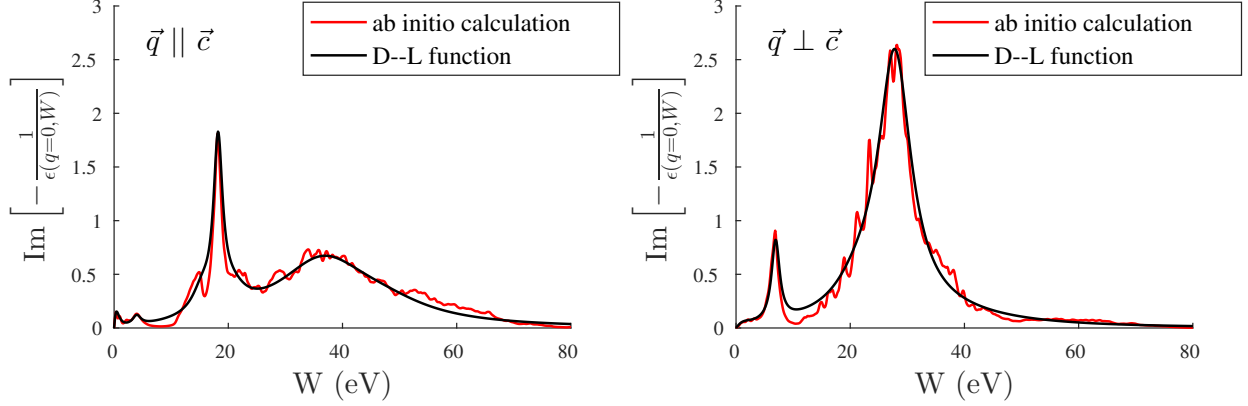


Figure 2: ELF functions along the two possible orthogonal directions of transferred momentum \vec{q} : *ab initio* calculations (red lines) are compared to the Drude–Lorentz best fits (black lines).

dispersion law obtained within the RPA⁶:

$$E_n(q \neq 0) = E_n(q = 0) + \frac{\hbar^2 q^2}{2m} \quad (5)$$

These data were used to compute the total inelastic scattering cross section σ_{inel} and the IMFP λ_{inel} by Eq. (2) (see Fig. 3).

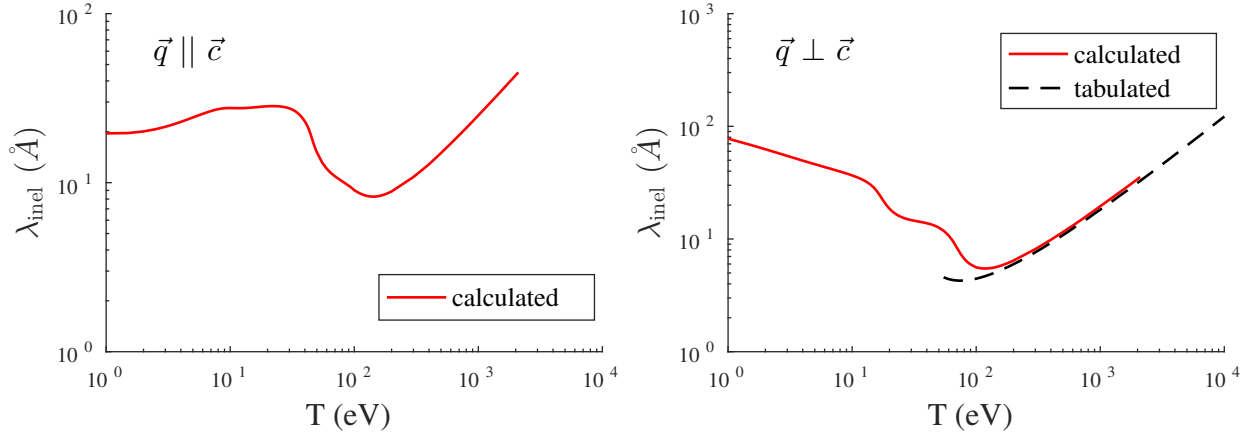


Figure 3: Inelastic mean free paths calculated along the two possible orthogonal directions of transferred momentum \vec{q} . In the case $\vec{q} \perp \vec{c}$ (right panel) the calculated values are compared with the data by Tanuma et al. (dashed lines)²⁰.

To calculate the total IMFP by taking into account the anisotropic structure of graphite, λ_{inel} and W were determined by linearly combining at each inelastic interaction the corre-

sponding values along the two possible orthogonal directions of the transferred momentum \vec{q} , as follows:

$$\lambda_{\text{inel}} = f \cos^2 \theta \lambda_{\parallel} + [(1 - f) + f \sin^2 \theta] \lambda_{\perp} \quad (6)$$

$$W = f \cos^2 \theta W_{\parallel} + [(1 - f) + f \sin^2 \theta] W_{\perp} \quad (7)$$

where f is an *anisotropy parameter* in the range $[0:1]$, and θ is the angle between \vec{c} and \vec{q} . The f parameter has been introduced in this anisotropic model of the inelastic observables to favour the electron motion in the planar direction, since HOPG shows a higher conductivity along the plane ($\vec{q} \perp \vec{c}$). The value of f is determined to obtain the best agreement between theoretical and experimental spectra.

Monte Carlo Model

Monte Carlo simulations were performed in order to interpret REEL and SE spectra of HOPG acquired in-house. Details on our Monte Carlo approach can be found in Ref.²¹.

To carry out Monte Carlo calculations some input information about the target material, such as atomic and mass number, density, elastic and inelastic mean free paths and probability distributions of elastic and inelastic scattering, is required. In particular, the characteristic quantities of the target material are: the atomic number ($Z = 6$), the atomic mass ($A = 12.011 \text{ uma}$)²², the density ($d = 2.25 \text{ g/cm}^3$)²³, the electronic band gap E_g (0.0 eV), and the work function ($WF = 4.6 \text{ eV}$)²⁴.

On the one hand, in the case of inelastic collisions the primary electrons lose their kinetic energy according to the cumulative probability distribution:

$$P_{\text{inel}}(T, W) = \lambda_{\text{inel}} \int_{E_g}^W \frac{d\lambda_{\text{inel}}^{-1}}{dW'} dW' \quad (8)$$

that depends on the initial kinetic energy T and on the energy loss W .

On the other hand, the change in the direction of the elastically scattered electrons can be

obtained by using the elastic cumulative probability:

$$P_{\text{el}}(T, \bar{\theta}) = \frac{2\pi}{\sigma_{\text{el}}} \int_0^{\bar{\theta}} \frac{d\sigma_{\text{el}}}{d\theta'} \sin \theta' d\theta' \quad (9)$$

that is determined for a fixed initial kinetic energy T by varying the scattering angle θ in the range $[0, \bar{\theta}]$. In Eq. (9) σ_{el} is the elastic scattering cross section.

Elastic and inelastic scattering probability distributions lead respectively to the assessment of the scattering angle and of the energy loss. Probability distributions were calculated at specific energies of the electrons, and in Tab. 3 we report both the electron kinetic energy ranges (E) and the relevant mesh intervals (ΔE) that we used in our MC simulations.

Table 3: Energy values at which scattering probabilities are calculated.

range	ΔE
$0 < E \leq 10$ eV	$\Delta E = 0.5$ eV
$10 < E \leq 50$ eV	$\Delta E = 1.0$ eV
$50 < E \leq 100$ eV	$\Delta E = 5.0$ eV
$100 < E \leq 200$ eV	$\Delta E = 10.0$ eV
$E \geq 200$ eV	$\Delta E = 100.0$ eV

Depending on the kinetic energy of the electron undergoing the collision, we select a probability distribution. The scattering angle (elastic interaction) or the energy loss (inelastic interaction) are determined by generating a random number, uniformly distributed in the interval $[0,1]$. In fact, (see Eq.(9)) the value of the elastic scattering cumulative probability (or of the inelastic scattering cumulative probability, see Eq. (8)) that equalizes this random number determines the scattering angle (or the energy loss). The total mean free path (λ), which characterizes the electron path in the target material is defined as:

$$\frac{1}{\lambda} = \frac{1}{\lambda_{\text{el}}} + \frac{1}{\lambda_{\text{inel}}} \quad (10)$$

where λ_{el} is the elastic mean free path. The probabilities of the elastic and inelastic events

can be evaluated, for any fixed value of kinetic energy and angle, as:

$$p_{\text{el}} = \frac{\lambda}{\lambda_{\text{el}}} \quad p_{\text{inel}} = \frac{\lambda}{\lambda_{\text{inel}}} \quad (11)$$

The decision on the type of collision that the electrons undergo is made by generating another random number uniformly distributed in the interval $[0,1]$. Whether this number is lower than p_{el} the interaction will be elastic, otherwise it will be inelastic. In Fig. 4 we report the elastic and inelastic collision probabilities as a function of the relevant variables θ and T .

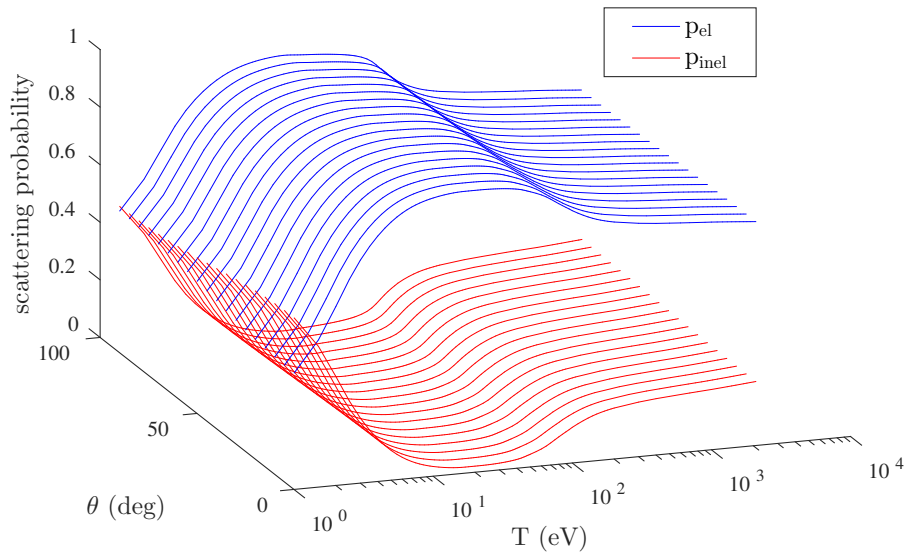


Figure 4: Collision probabilities as a function of the electron kinetic energy (T) and of the angle (θ) between the transferred momentum \vec{q} and the vector \vec{c} normal to the surface.

Results and Discussion

REELS

Different simulations were carried out at several beam kinetic energies to simulate our recorded REEL spectra. In the Monte Carlo runs, the trajectories of $N = 10^9$ primary electrons were followed in order to achieve a good statistics. The beam incidence angle was fixed at 30° with respect to the normal to the surface, according to our experimental

conditions. First, we investigated the dependence of the REEL spectra on the parameter f by spanning a range of possible values in Eqs. (6) and (7). Fig. 5 compares the REEL theoretical spectra (red lines), obtained for an initial kinetic energy of 1500 eV, at different values of f with our experimental data (black lines).

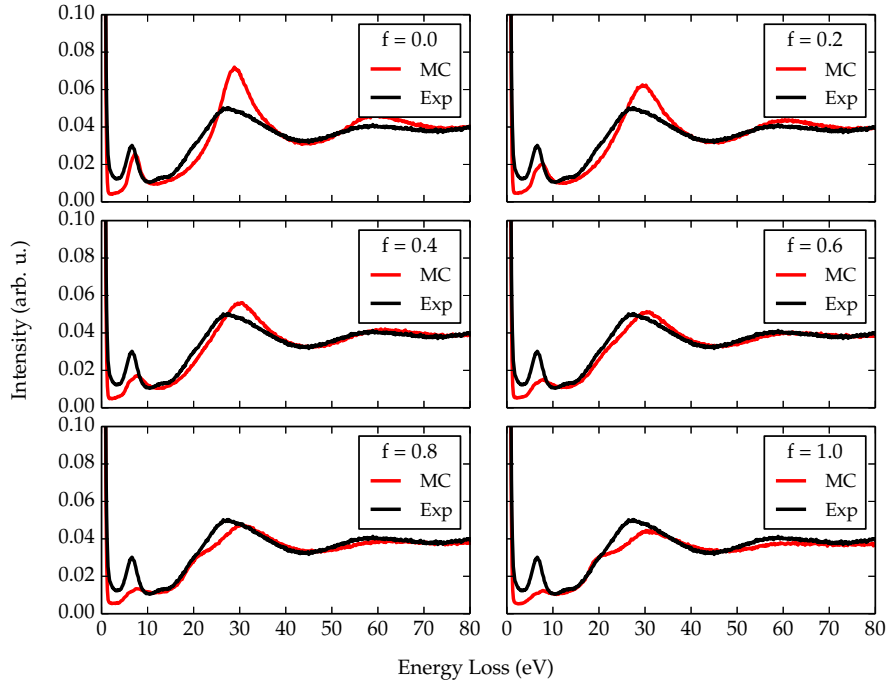


Figure 5: REELs of HOPG for different values of the f parameter (red lines). The kinetic energy of the primary beam is set to 1500 eV. MC calculations are compared with our experimental data (black lines)²¹. The spectra are normalized at a common area of the elastic peak.

The higher the value of f , the larger is the contribution of intra-planar excitations ($\vec{q}||\vec{c}$) to inelastic interactions. This effect can be noticed in the spectra of Fig. 5 by the rise of a shoulder at an energy loss of 20 eV, which corresponds to an oscillation in the ELF along the $\vec{q}||\vec{c}$ direction. The value of the anisotropy parameter that shows the best agreement between experimental and calculated REELS normalized at a common area of the elastic peak is $f = 0.6$. Indeed, by performing a chi-squared test in the energy loss range [-2:80] eV, the lowest value of the χ^2 can be obtained using $f = 0.6$ (see table 4). Nevertheless, a value equal to 0.6 of this anisotropic parameter delivers the best agreement also in other

primary beam energy ranges. Thus, we set the anisotropy parameter to this value in all MC simulations. This means physically that by considering e.g. a scattering angle $\theta = 0^\circ$

Table 4: χ^2 -test carried out by considering the experimental and calculated data normalized at a common area of the elastic peak in the energy loss range [-2:80] eV for different values of the parameter f .

f	χ^2
0.0	134
0.2	207
0.4	125
0.6	93
0.8	95
1.0	174

(that is, orthogonal to the graphite layers), the energy loss embeds 60% of collisions with a transferred momentum along the $\vec{q}||\vec{c}$ direction, while 40% of the spectrum is made by collisions along the $\vec{q}\perp\vec{c}$ (in-plane) direction (Eqs. (6) and (7)). Of course, the directional change of the electrons inelastically scattered by the target nuclei is taken into account, for fixed f , by the scattering angle θ , which is modified by the interactions at each MC step. This anisotropic model is consistent with the higher tendency of the electrons to move along the graphite planes rather than across the planes.

MC simulations were performed at several primary beam kinetic energies and compared with our experimental data (normalized at a common area of the elastic peak) in Fig. 6.

We notice that the agreement between calculated and experimental data is rather good and becomes progressively better for increasing kinetic energies. This is due to the fact that our experimental spectra report also the contribution of surface plasmons, which is neglected in the MC calculations and whose relative importance diminishes with respect to bulk plasmons at higher values of the primary beam kinetic energy. It is worth noting that the normalization of the data at a common area of the elastic peak keeps the correct intensity ratios between the two main plasmon peaks.

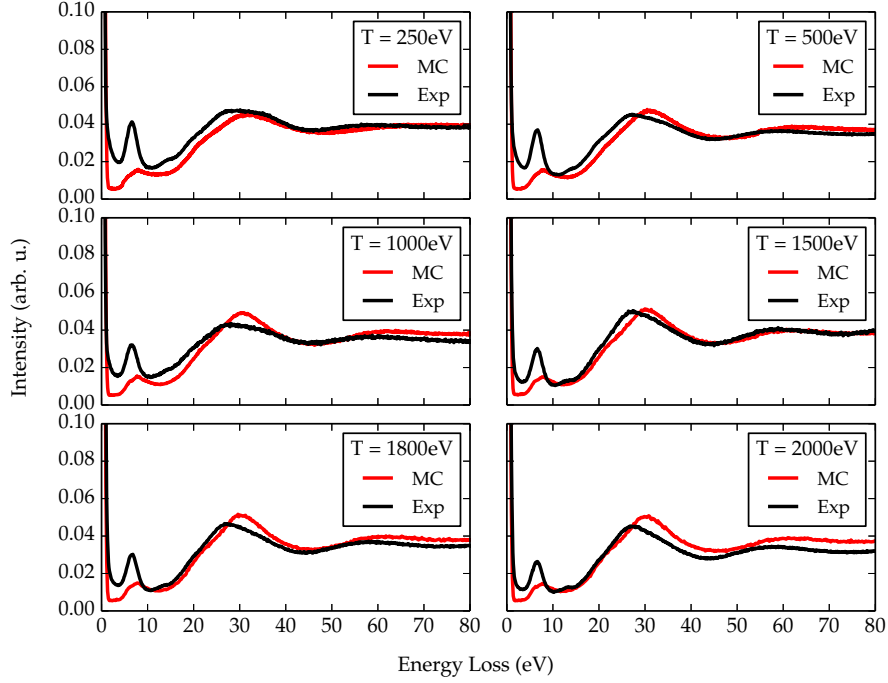


Figure 6: REELs of HOPG for several primary beam kinetic energies. Red lines show simulated spectra, while black curves report our experimental data²¹. The results are normalized at a common area of the elastic peak.

Secondary Electron Spectrum

A quantitative understanding of SE spectra is crucial in imaging techniques. SE emission from graphite was thus assessed by MC simulations, using a kinetic energy of the incident beam ($N = 10^6$) equal to 1000 eV. In the MC simulations the beam incident direction was chosen orthogonal to the sample surface, according to our experimental conditions (see experimental details section). In Fig. 7 we compare our MC calculations with the acquired experimental spectra. While the shape of the theoretical and experimental SE spectra is comparable, however the simulated spectrum has been shifted by 0.7 eV along the positive axis direction, in order to align the dominant emission peak.

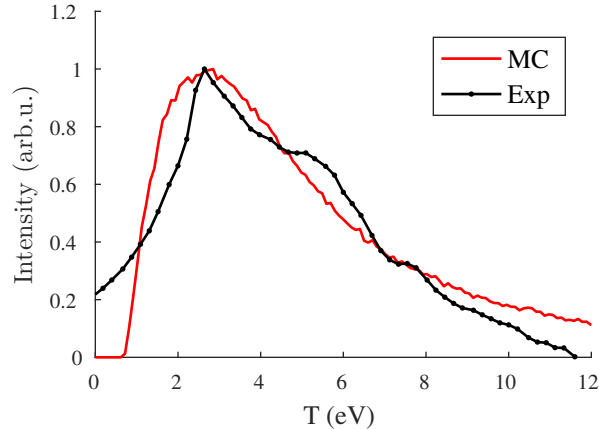


Figure 7: Secondary electron spectra of HOPG. Black lines represent experimental data, while in red we report the theoretical spectrum. The data are normalized to a common height of the secondary electron emission peak.

Conclusions

In this work, we performed Monte Carlo simulations, based on ab-initio input data of the energy-dependent dielectric function, of REEL and SE spectra of graphite, taking into account features related to the anisotropic structure of the target material. Graphite has indeed a layered structure and this must be considered in the treatment of the electron transport properties. In particular, the determination of the inelastic mean free path and of the energy loss was carried out by considering a linear combination of the dielectric properties along the two main orthogonal crystal directions (in-plane and out of plane). In our model, coefficients of this linear combinations depend on an anisotropy parameter f and on the angle between the transferred momentum \vec{q} and the surface normal vector \vec{c} . Our approach for including a dependence of the dielectric properties on the target anisotropy clearly improves the agreement between simulated and experimental REEL spectra. Indeed, spectral features are well reproduced by MC calculations for a value of the anisotropy parameter $f = 0.6$. This means that the energy loss along the $\vec{q}||\vec{c}$ (inter-planar) direction contributes for 60% of inelastic collisions, while 40% of the spectral features are contributed by collisions along the $\vec{q}\perp\vec{c}$ direction (in-plane). Furthermore, the MC simulations of secondary emission spectra, whose quantitative understanding is important in imaging applications, were carried out

by using our anisotropic model and compared to in-house recorded experimental spectra. We found a good agreement between theoretical and acquired spectra with respect to the lineshape, that is the intensity of the spectral features, while an energy shift was imposed to the theoretical data to reproduce the energy of the main emission peak. These findings demonstrate the importance of considering properly-weighted inter-planar and intra-planar interactions in the simulation of charge transport in layered materials. Finally, the accuracy of our approach can be tested and possibly improved by considering other descriptions of the ELF at low energies, such as using the Mermin dielectric function presented by Garcia-Molina et al. in Ref.²⁵. Moreover, the performance of these models in the optical limit can be further improved by taking into account more rigorously the exchange-correlation effects, particularly at low energy, according to Emfietzoglou et al.^{26,27}.

Acknowledgement

N.M.P. is supported by the European Commission H2020 under the Graphene Flagship Core 1 No. 696656 (WP14 "Polymer Composites") and under the FET Proactive "Neurofibres" No. 732344. S.T acknowledge funding from No. 696656 WP14 "Polymer Composites" grant. C.R. was funded by EPSRC (EP/N008065/1). Access to computing and storage facilities owned by parties and projects contributing to the National Grid Infrastructure MetaCentrum provided under the program "Projects of Large Research, Development, and Innovations Infrastructures" (CESNET LM2015042), is greatly appreciated (<https://www.metacentrum.cz/en/>). The authors gratefully acknowledge the Gauss Centre for Supercomputing for funding this project by providing computing time on the GCS Supercomputer JUQUEEN at Jülich Supercomputing Centre (JSC)²⁸. Furthermore, the authors acknowledge FBK for providing unlimited access to the KORE computing facility.

References

- (1) Taioli, S.; Umari, P.; De Souza, M. M. Electronic properties of extended graphene nanomaterials from GW calculations. *Physica Status Solidi (B)* **2009**, *246*, 2572–2576.
- (2) Umari, P.; Petrenko, O.; Taioli, S.; Souza, M. M. D. Communication: Electronic band gaps of semiconducting zig-zag carbon nanotubes from many-body perturbation theory calculations. *The Journal of Chemical Physics* **2012**, *136*, 181101.
- (3) Krishnan, N., K Sand Ganguli Large Anisotropy of the Electrical Conductivity of Graphite. *Nature* **1939**, *144*, 667.
- (4) Mott, N. The scattering of fast electrons by atomic nuclei. *Proceedings of the Royal Society of London. Series A, Containing Papers of a Mathematical and Physical Character* **1929**, *124*, 425.
- (5) Ritchie, R. H. Plasma Losses by Fast Electrons in Thin Films. *Phys. Rev.* **1957**, *106*, 874.
- (6) Nikjoo, H.; Emfietzoglou, D.; Liamsuwan, T.; Taleei, R.; Liljequist, D.; Uehara, S. Radiation track, DNA damage and response: a review. *Reports on Progress in Physics* **2016**, *79*, 116601.
- (7) Young, R.; Bosch, E.; Uncovsky, M.; Tuma, L. Low-energy secondary electron filtering with immersion lens SEM. *Microscopy and Microanalysis* **2009**, *15*, 222.
- (8) Wan, Q.; Abrams, K.; Masters, R.; Talari, A.; Rehman, I.; Claeysens, F.; Holland, C.; Rodenburg, C. Mapping Nanostructural Variations in Silk by Secondary Electron Hyperspectral Imaging. *Advanced Materials* **2017**,
- (9) Willis, R.; Feuerbacher, B.; Fitton, B. Graphite conduction band states from secondary electron emission spectra. *Physics Letters A* **1971**, *34*, 231–233.

- (10) Hoffman, A. Fine structure in the secondary electron emission spectrum as a spectroscopic tool for carbon surface characterization. *Diamond and Related Materials* **1994**, *3*, 691–695.
- (11) Dapor, M. *Transport of Energetic Electrons in Solids*; Springer Tracts in Modern Physics, 2017.
- (12) Taioli, S.; Simonucci, S. In *Chapter Five - A Computational Perspective on Multichannel Scattering Theory with Applications to Physical and Nuclear Chemistry*; Dixon, D. A., Ed.; Annual Reports in Computational Chemistry; Elsevier, 2015; Vol. 11; pp 191 – 310.
- (13) Taioli, S.; Simonucci, S.; Calliari, L.; Dapor, M. Electron spectroscopies and inelastic processes in nanoclusters and solids: Theory and experiment. *Physics Reports* **2010**, *493*, 237 – 319.
- (14) Taioli, S.; Simonucci, S.; Dapor, M. SURPRISES: when ab initio meets statistics in extended systems. *Computational Science and Discovery* **2009**, *2*, 015002.
- (15) Taioli, S.; Simonucci, S.; Calliari, L.; Filippi, M.; Dapor, M. Mixed ab initio quantum mechanical and Monte Carlo calculations of secondary emission from SiO₂ nanoclusters. *Phys. Rev. B* **2009**, *79*, 085432.
- (16) <http://elk.sourceforge.net/>.
- (17) Dapor, M. Elastic scattering calculations for electrons and positrons in solid targets. *Journal of Applied Physics* **1996**, *79*, 8406.
- (18) Dapor, M.; Masters, R. C.; Ross, I.; Lidzey, D. G.; Pearson, A.; Abril, I.; Garcia-Molina, R.; Sharp, J.; Unčovský, M.; Vystavel, T. Secondary electron spectra of semi-crystalline polymers—A novel polymer characterisation tool? *Journal of Electron Spectroscopy and Related Phenomena* **2018**, *222*, 95–105.

- (19) Ganachaud, J.; Mokrani, A. Theoretical study of the secondary electron emission of insulating targets. *Surface Science* **1995**, *334*, 329.
- (20) Tanuma, S.; Powell, C.; Penn, D. Calculations of electron inelastic mean free paths. IX. Data for 41 elemental solids over the 50 eV to 30 keV range. *Surface and Interface Analysis* **2011**, *43*, 689.
- (21) Azzolini, M.; Morresi, T.; Garberoglio, G.; Calliari, L.; Pugno, N. M.; Taioli, S.; Dapor, M. Monte Carlo simulations of measured electron energy-loss spectra of diamond and graphite: Role of dielectric-response models. *Carbon* **2017**, *118*, 299.
- (22) <http://www.rsc.org/periodic-table/element/6/carbon>.
- (23) Garcia-Molina, R.; Abril, I.; Denton, D.; Heredia-Avalos, S. Allotropic effects on the energy loss of swift H^+ and He^+ ion beams through thin foils. *Nuclear Instruments and Methods in Physics Research Section B: Beam Interactions with Materials and Atoms* **2006**, *249*, 6 – 12.
- (24) Zhou, Y.; Fox, D. S.; Maguire, P.; OConnell, R.; Masters, R.; Rodenburg, C.; Wu, H.; Dapor, M.; Chen, Y.; Zhang, H. Quantitative secondary electron imaging for work function extraction at atomic level and layer identification of graphene. *Scientific reports* **2016**, *6*, 21045.
- (25) Garcia-Molina, R.; Abril, I.; Kyriakou, I.; Emfietzoglou, D. Inelastic scattering and energy loss of swift electron beams in biologically relevant materials. *Surface and Interface Analysis* **2017**, *49*, 11–17.
- (26) Emfietzoglou, D.; Kyriakou, I.; Garcia-Molina, R.; Abril, I. Inelastic mean free path of low-energy electrons in condensed media: beyond the standard models. *Surface and Interface Analysis* **2017**, *49*, 4–10.

- (27) Emfietzoglou, D.; Kyriakou, I.; Garcia-Molina, R.; Abril, I. The effect of static many-body local-field corrections to inelastic electron scattering in condensed media. *Journal of Applied Physics* **2014**, *114*, 144907.
- (28) Jülich Supercomputing Centre, JUQUEEN: IBM Blue Gene/Q Supercomputer System at the Jülich Supercomputing Centre. *Journal of large-scale research facilities* **2015**, *1*.